Helium Cryogenics

Steven W. Van Sciver
University of Wisconsin–Madison
Madison, Wisconsin

PLENUM PRESS • NEW YORK AND LONDON

Library of Congress Cataloging in Publication Data

Van Sciver, Steven W.
Helium cryogenics.

(International cryogenics monograph series)
Includes bibliographies and index.
1. Liquid helium. 2. Helium at low temperatures. I. Title. II. Series.
QC145.45.H4V36 1986 536'.56 86-20461
ISBN 0-306-42335-9

10 9 8 7 6 5 4 3

Chapter 5

He II Heat Transfer

Chapter 4 emphasized the physical understanding of He II including heat transport in the laminar flow and turbulent mutual friction regimes. These mechanisms are fundamental to the behavior of He II, although they represent rather idealized conditions. Therefore, it is of interest to apply the treatment of He II to practical heat transfer problems. In doing so, the concepts already developed must be extended into regimes that are usable in more practical situations. To be more specific, the emphasis of Chapter 4 has been to understand the interactive mechanisms. Thus, of principal concern are the behavior of the transport properties including mainly the normal fluid viscosity η_n and the mutual friction parameter A. Of interest now is to use these concepts in understanding such phenomena as the maximum heat flux q^*, the maximum energy deposition ΔE^*, and the maximum temperature difference ΔT_m, which can be either within the fluid or across a solid–fluid interface. The goal of the present chapter is to establish a connection between the engineering parameters q^*, ΔE^*, and ΔT_m and the physical properties of the fluid and solid–fluid boundaries. In establishing this connection there are a number of subjects of practical interest which must be addressed. These include steady-state heat transport, forced convection, transient heat transport, Kapitza thermal boundary conductance, and film boiling. Some of these phenomena are also important in pool boiling He I heat transfer, which is the subject of Chapter 6.

Before delving into these individual subjects, it is worth describing, in a general way, the heat transfer character of liquid He II. This character in fact does not deviate qualitatively from that of He I, albeit the numerical values and physical explanation are considerably different. A typical steady-state heat transfer curve for a metal surface at the end of a duct containing He II is plotted in Fig. 5.1. These results are intended only to display the regions of heat transfer. As is demonstrated in what follows, actual numerical values of these regimes are strongly dependent on geometry, temperature, pressure, and surface conditions. For small ΔT up to q^*, the

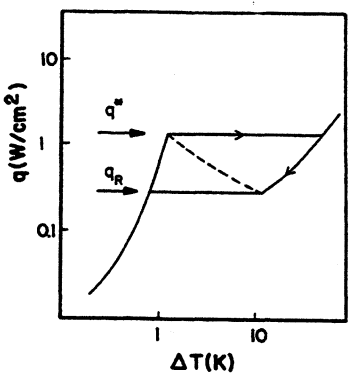

Fig. 5.1. A typical steady-state heat transfer curve for a metal surface at the end of a duct containing He II.

surface temperature difference is governed by interfacial phenomena having more to do with the character of the solid than that of the liquid helium. This is called the Kapitza regime. There is no boiling occurring, rather the temperature difference is a result of thermal impedance between the two dissimilar materials, the metal or insulating solid and liquid He II. The maximum heat flux q^* is strongly geometry and helium state dependent. It is characterized by the point where the helium adjacent to the interface exceeds the local boiling point. The maximum heat flux is also time dependent, achieving very high values for short-duration heat pulses. Once this maximum is exceeded, the heat transfer converts to a film boiling process where a film consisting of either He I, vapor, or both blankets the surface. Finally, in some configurations there is observed a hysteresis in the heat transfer curve exemplified by the requirement to reduce q below q^* to return to the Kapitza regime. This process is reasonably well understood in He I, being given by an engineering correlation. However, in He II the problem is more complex and has received less attention, owing to the experimental difficulty of achieving steady state and strong variations with configuration. It is the physical understanding of this heat transfer curve that is the goal of the present chapter. The description is based heavily on the heat transport modeling of He II contained in Chapter 4.

5.1. STEADY-STATE HEAT TRANSPORT

The first question to ask is: What are the limitations to heat transport in a channel containing He II? Since the heat transport equations for He II have already been developed, it should be straightforward to apply these equations to determine practical limitations. In doing so, it is assumed that the heat transport equations can be applied much the same as Fourier's law is applied to heat conduction in a solid. Note that He II cannot exist

above the λ-transition, 2.172 K at SVP, which at least establishes temperature boundaries to the heat transfer problem. For a channel of finite length L, as shown in Fig. 5.2, subjected to a constant heat flux q, there is a temperature difference established across its length, that is $\Delta T = T_m - T_b$. In general, this temperature difference occurs because of two mechanisms, normal fluid viscous interactions with the boundaries and mutual friction between the two fluid components. Since most practical applications call for channel diameters and heat fluxes that are sufficiently large to allow the mutual friction term to dominate, the normal fluid viscous interaction will be neglected throughout this discussion. It is equally straightforward, in principle, to solve the steady-state heat transport problem including the normal fluid viscous term, although the mathematics are more cumbersome.

5.1.1. Peak Heat Flux in Wide Channels

The turbulent heat transport equation in one dimension is written in the form

$$\frac{dT}{dx} = -f(T)\, q^m \tag{5.1}$$

where $f(T) = A\rho_n/(\rho_s^3 s^4 T^3)$ and m is a numerical coefficient which theory indicates should be equal to 3 but which experimentally has been shown to vary from below 3 to nearly 4 as the temperature approaches T_λ.[1-3] Recall that A is the Gorter–Mellink mutual friction parameter and ρ_n and ρ_s are the normal and superfluid densities, respectively. The origin of (5.1) is discussed extensively in Section 4.5. The quantity $f^{-1}(T)$ behaves much like a thermal conductivity in that it is a fluid property that controls the temperature gradient in the presence of a heat flux. It is therefore of interest to understand the variation of $f^{-1}(T)$ with the state of the helium. Plotted in Fig. 5.3 is this function as it depends on temperature and pressure between 1.4 K and T_λ and p = SVP and 2.5 MPa. Note that the temperature dependence is quite strong with a maximum occurring around $T = 1.9$ K at SVP. The pressure dependence is weaker and somewhat uncertain owing to the limited quantity of data available for the pressure dependence of the Gorter–Mellink parameter. In the data presented in Fig. 5.3, Vinen's[1] values for

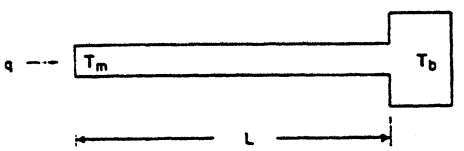

Fig. 5.2. Schematic of a channel containing He II.

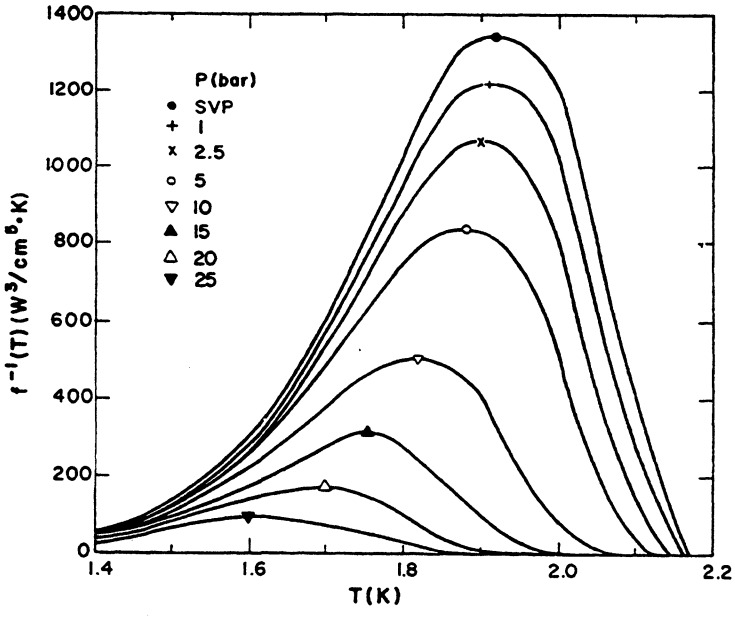

Fig. 5.3. Heat conductivity function for turbulent He II. Symbols indicate the location of the peak value.

the Gorter–Mellink parameter have been used. Furthermore, it has been assumed that $A\alpha\rho_n^2/\rho^3$, which is based on theory[4] and supported to some extent by experiment.[3] Based on an empirical fit to the Gorter–Mellink parameter, it is also possible to write an analytic expression for the heat conductivity function,

$$f^{-1}(T, p) = g(T_\lambda)[t^{5.7}(1 - t^{5.7})]^3 \tag{5.2}$$

where $g(T_\lambda) = \rho^2 s_\lambda^4 T_\lambda^3 / A_\lambda$, $t = T/T_\lambda$, $S_\lambda = 1.559$ J/gm·K, and $A_\lambda \simeq$ 145 cm·sec. Note that at saturated vapor pressure, the maximum in (5.2) occurs at 1.923 K, which is generally consistent with experiment. The values presented in Fig. 5.3 are good to about ±10% at saturated vapor pressure and have been compared to experiment up to about 7 bars.[5] At this time results are not available at higher pressures.

If the interest is in the heat transport in a finite-length channel with a sizable ΔT, it is possible to determine its value by integration of (5.1) and matching boundary conditions. The maximum heat flux q^* is then established according to the maximum allowable temperature difference

across the channel, which for a given bath temperature T_b is $(T_\lambda - T_b)$. It follows that for a channel of length L

$$q^* = \left(\frac{1}{L}\int_{T_b}^{T_\lambda} \frac{dT}{f(T)}\right)^{1/m} \tag{5.3}$$

where for $m = 3$, the heat conductivity function is given in (5.2). This integral is mostly a function of T_b and only weakly dependent on other factors such as pressure. It is possible to define a function of the form

$$q^* L^{1/m} \equiv Z(T_b) = \left(\int_{T_b}^{T_\lambda} \frac{dT}{f(T)}\right)^{1/m} \tag{5.4}$$

which should be independent of channel length. Plotted in Fig. 5.4 are experimentally determined peak heat fluxes q^* for different channel lengths varying everywhere from 0.1 to 3 m. Two different correlations of the data are displayed: one for $m = 3$ and the other for $m = 3.4$. In either case, the agreement between data and correlation is quite acceptable.

A similar analysis is possible to determine the pressure dependence of the maximum heat flux q^*. Integration of the corresponding heat conductivity function $f^{-1}(T, p)$ predicts a decreasing maximum heat flux with elevated pressure. By analytic integration of (5.2), a prediction can be made for the behavior of q^* with pressure. The results of this analysis for four bath temperatures are displayed in Fig. 5.5. Also displayed are experimentally observed[3,6] maximum heat fluxes for short channels up to 0.3 MPa. The agreement is reasonable for the available data.

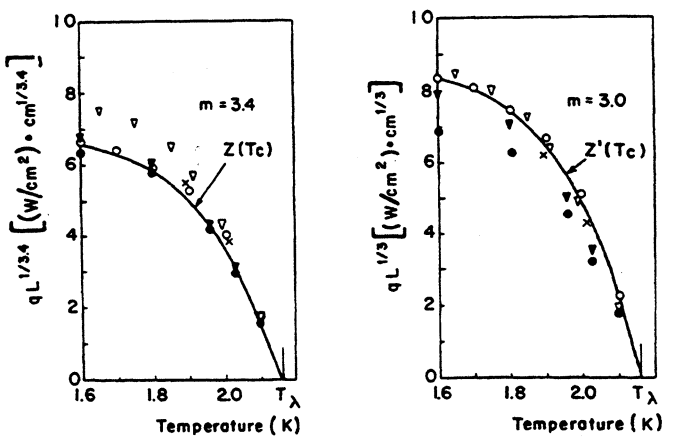

Fig. 5.4. Generalized steady-state limiting heat flux in He II (as compiled by Seyfert[60]).

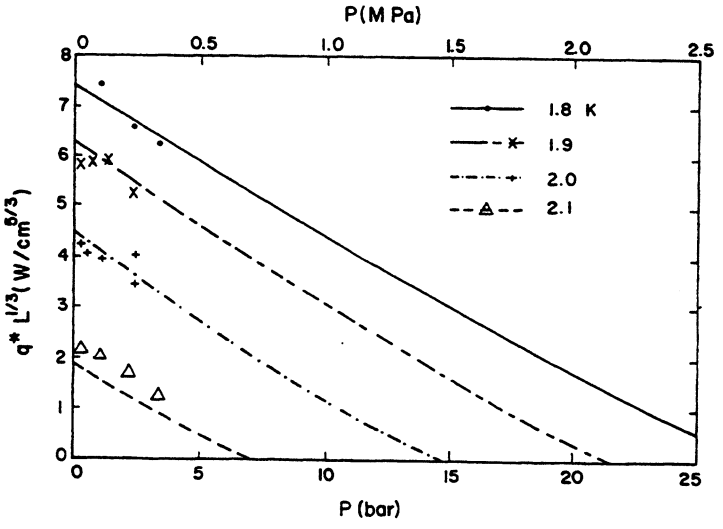

Fig. 5.5. Maximum heat flux in a He II-containing channel as a function of pressure (data from Ref. 3 and 6).

It should be kept in mind that the form and physical explanation for heat transport in He II place no fundamental limit to the maximum steady-state value for q^*. Everything depends on the allowable temperature difference. For example, with $T_b = 1.8$ K and $m = 3$, Fig. 5.4 predicts a product $q^* L^{1/3} = 7.4$ W/cm$^{5/3}$. Therefore, for a channel of length 10 μm, this analysis would predict a q^* in excess of 70 W/cm^2, truly a remarkable heat flux for liquid helium temperatures.

5.1.2. Peak Heat Flux in Cylindrical Geometries

Besides the simple linear geometry represented by a one-dimensional tube with constant heat flux, there has been considerable work carried out on cylindrical geometries consisting of a heated cylinder or wire immersed in a large bath of He II.[7-10] It is easy to show,[11] by assuming that the Gorter–Mellink equations apply in cylindrical geometry, that the steady-state heat transport equation can be written

$$\frac{dT}{dr} = f(T)\, q_0^m \left(\frac{r_0}{r}\right)^m \tag{5.5}$$

where q_0 is the heat flux per unit area of the heated cylinder of radius r_0. The difference in (5.5) occurs because the heat flux decreases as the radius increases. Comparison of (5.5) with experiment has given reasonable

agreement, with essentially the same heat conductivity function as applies in linear geometries.[10,11] In a similar fashion to that applied to (5.3), integration of (5.5) leads to the maximum heat flux,

$$q_0^* = \left(\frac{m-1}{r_0}\int_{T_b}^{T_\lambda}\frac{dT}{f(T)}\right)^{1/m} \tag{5.6}$$

The important observation to make about (5.6) is that the peak heat flux q_0^* has as its scaling length r_0 rather than L as in the linear system. This means that, provided the radius of the container is much larger than that of the heater, the boundary conditions far from the heater should not affect q^* significantly. This is certainly contrary to the behavior in linear geometries.

Unlike the linear one-dimensional system, there have been fewer attempts to correlate the peak heat transport in cylindrical geometries with that of (5.6). This is due in part to the lack of reliable data, which are more difficult to obtain in cylindrical geometries. One such effort made use of data for small temperature differences $\Delta T \approx 10\,\text{mK}$ in the range of $T_b = 1.8\,\text{K}$. It was found that the expression given by (5.6) is not entirely suitable to correlate the experimental values of q_0^* without introducing a radius-dependent quantity ψ defined by

$$q_0^* = \left(\frac{2\psi}{r_0}\int_{T_b}^{T'}\frac{dT}{f(T)}\right)^{1/3} \tag{5.7}$$

where $T' \simeq T_b + 0.01\,\text{K}$. ψ was found empirically to depend on radius, being roughly proportional to $r_0^{1/2}$. The results of this correlation are shown in Fig. 5.6. Note that ψ is always less than 1, indicating that the peak heat flux is always less than that predicted by the idealized theory. This fact is somewhat surprising because the temperature gradients appear to be given accurately by (5.5).[11]

5.1.3. Peak Heat Flux in Saturated He II

Until now, it has been assumed arbitrarily that the peak heat flux q^* is determined by the condition that the helium adjacent to the heater surface reaches the λ-point. This condition does not always occur for reasons having to do with the helium temperature distribution and the phase diagram, displayed in Fig. 5.7. First of all, because of the high effective thermal conductivity of He II, it is reasonable to assume that the helium within the heat transfer region obeys equilibrium thermodynamics. This

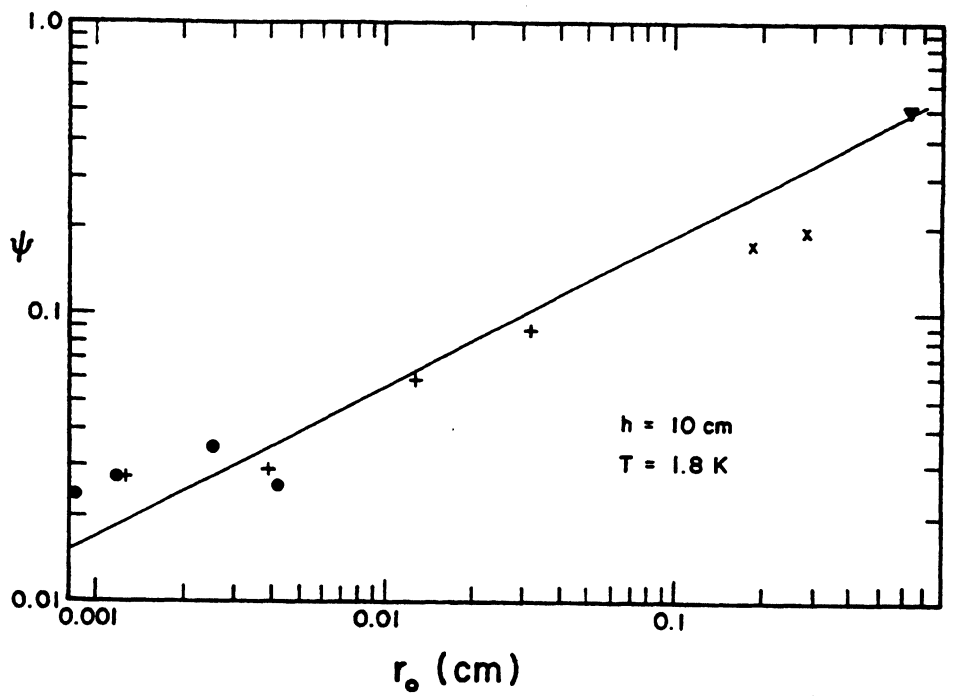

Fig. 5.6. Empirical correlating function for heat transfer in cylindrical geometries (data from references 8–10).

assumption allows the state of the helium everywhere in an experiment or engineering system to be described by a point on the phase diagram.

Now consider a simple example, that of a heat transfer experiment in a saturated bath of liquid helium boiling at 1.8 K, 1.6 kPa (12.5 torr). The process is occurring at a certain depth below the liquid–vapor interface; see Fig. 5.8. Thus, without any heat being applied, the state of the helium can be described by location ① on the phase diagram in Fig. 5.7. The pressure applied at the heat transfer surface is therefore $p = p_0 + \rho gh$, where h is the hydrostatic head of the liquid helium. If heat is applied to induce heat transfer in the system, there will be a local temperature excursion ΔT that is determined by heat flow mechanisms. The local temperature increases but the pressure is fixed, unless the experimental configuration is small enough for the thermomolecular effect to make a significant contribution. Avoiding this complication for the time being, we see that the temperature will follow a horizontal line as shown in the inset of Fig. 5.7 until it meets the liquid–vapor interface at which point boiling commences. The value of the maximum temperature excursion is determined by the slope of the vapor pressure curve:

$$\Delta T_m = \int_{p_0}^{p_0 + \rho gh} \left(\frac{dT}{dp}\right) dp \tag{5.8}$$

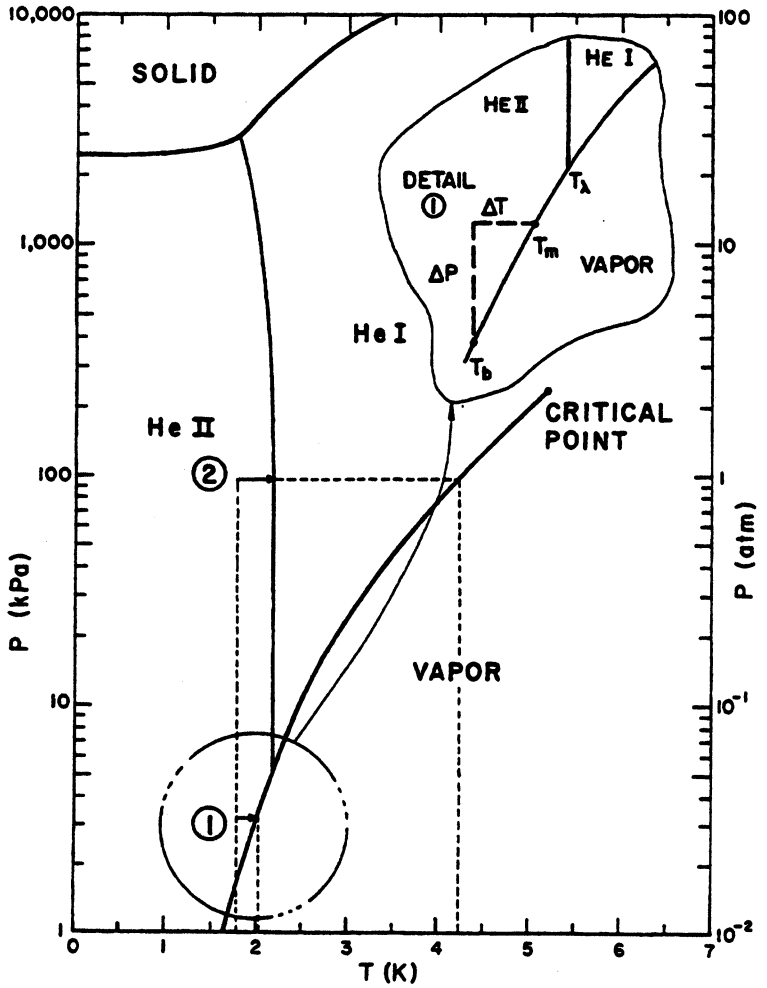

Fig. 5.7. Phase diagram of helium showing location ① of near saturation conditions and location ② of subcooled conditions.

The slope of the vapor pressure curve, dT/dp, is known through the Clausius–Clapeyron equation,

$$\frac{dp}{dT} = \frac{\lambda}{T\,\Delta v} \approx \frac{\lambda}{T v_g} \tag{5.9}$$

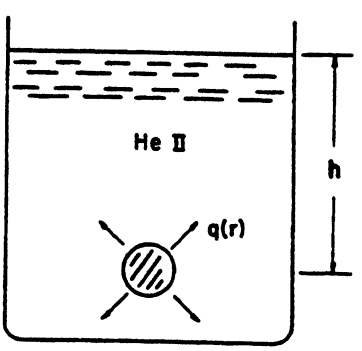

Fig. 5.8. Idealized heat transfer experiment in near-saturated He II.

and assuming the helium vapor to be an ideal gas, that is $v_g = RT/p$, we can approximate by

$$\Delta T_m \simeq \frac{RT^2}{\lambda} \ln\left(1 + \frac{\rho g h}{p_0}\right) \tag{5.10}$$

This expression is suitable for $\Delta T_m \ll T_b$. For larger values of ΔT it is better to evaluate the saturation temperature at the pressure corresponding to the given hydrostatic head. This can be achieved most easily by using tabulated values for vapor pressure.[12]

As an aside it is worth mentioning that the above description is not without controversy. In fact, a number of studies[13–15] have attempted to demonstrate experimentally the existence of superheated liquid in saturated He II. However, all these experiments have been performed using He II contained within a duct. The difficulty here is that the time constant for the steady state in this geometry can be quite long, leading to the belief that the observed superheat may be metastable. The resolution of this dilemma will have to wait for future work in this area.

To attach some quantitative understanding to the above discussion, it is worth noting that the pressure corresponding to the λ-point is $p_\lambda = 4.97$ kPa (37 torr), which is equivalent to a column of helium about 3.55 m high. This fact is important because if a He II system with vertical dimension larger than several meters is constructed, it would experience a heat transfer limitation determined by the He II–He I phase transition. Alternatively, it is possible to create a condition whereby the pressure at the heat transfer surface is arbitrarily high. This can occur in a closed-volume He II region cooled by a heat exchanger to a saturated bath. The pressure on the closed volume can therefore take on any value between saturation and 2.5 MPa.

The subcooled He II state is shown on th phase diagram by position ②. Here it is assumed, for example, that the applied pressure is 100 kPa (1 bar). A similar argument to that presented above applies when determining the temperature excursion; however, in the subcooled case the maximum temperature is governed by the λ-transition (at $p = 100$ kPa, $T_\lambda = 2.163$ K). Thus, the limits are relatively well fixed and only weakly dependent on applied pressure.

The conditions that exist once the maximum heat flux is exceeded are of great importance to understanding the heat transfer in this regime. Generally, there are two cases that can occur, each of which is associated with one of the two conditions indicated on the phase diagram in Fig. 5.7. For the saturation case which applies to position ①, q^* corresponds to the helium adjacent to the interface achieving saturation conditions. A schematic representation of the resulting physical condition for $q > q^*$ is

shown in Fig. 5.9a. Displayed is a solid heat transfer surface blanketed by a vapor film which in turn is bounded by the He II at local saturation temperatures. This phase boundary is defined clearly because the He II–vapor transition is first order.

The alternative film boiling heat transfer situation occurs whenever q^* is exceeded under subcooled conditions, such as ② in Fig. 5.7. For this case the phase transition is between He II and normal liquid He I. Since, with rare exception, the maximum heat flux in He I is substantially less than that in He II, exceeding q^* under subcooled conditions invariably results in a double transition, first creating a film of liquid He I followed by boiling of the He I to form a vapor film. This triple-phase phenomenon brings all three helium states in close proximity to the heat transfer interface. A schematic representation of this process is shown in Fig. 5.9b. Through the He II–He I interface, shown as a dotted line in the figure, the density ρ and temperature T should be continuous. Recent visual experiments of boiling in saturated and subcooled He II have allowed observation of the interfaces between the vapor–He I and the He I–He II phases.[16] The latter observation is particularly significant since the physical properties of helium should be continuous through the interface.

5.1.4. Forced Convection Heat Transfer

The subject of steady-state heat transport would not be complete without some discussion of the effect of forced convection on the temperature gradient and peak heat flux. This subject is a somewhat more general heat transport problem than has been considered so far because it includes an additional variable, the net flow velocity v. Forced convection was introduced in Chapter 4 as part of the two-fluid model applied to He II heat transport.

Since there have been fewer experimental investigations relating to forced flow He II heat transport, the analysis of the problem is incomplete. A general configuration to consider is shown in Fig. 5.10. A channel of constant cross section and length L connects two reservoirs at temperatures T_1 and T_2. Steady-state heat is applied to one end of the channel and the temperature difference is established, ultimately leading to the peak heat flux q^*. In fact, this configuration is not easily obtainable because a tem-

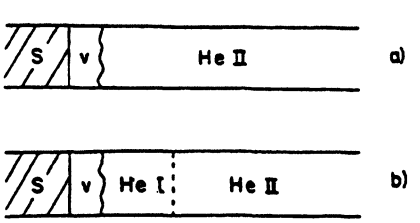

Fig. 5.9. Schematic of boiling in He II: (a) saturation condition and (b) subcooled condition.

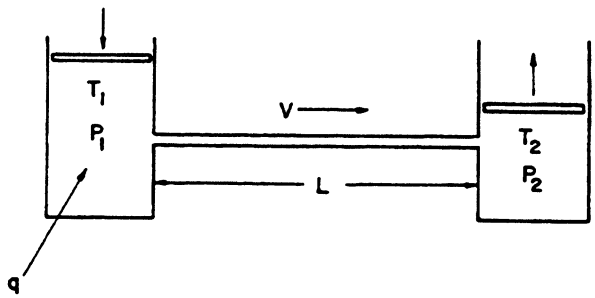

Fig. 5.10. Schematic representation of configuration required to obtain forced flow He II.

perature difference normally corresponds to a pressure difference under saturation conditions. However, it is possible to create the appropriate circumstances with a frictionless, massless piston that forces the liquid from volume 1 to volume 2 at velocity v.

To treat the problem of forced flow He II analytically, it is necessary to solve the heat balance equation that describes the system of interest.[17] In developing this equation, two fundamental assumptions are made about the physical behavior of He II. These assumptions are not proved here but are justified by the analysis of experimental data.

The first assumption is that the heat flow by internal convection mechanisms is not affected by the net velocity of the fluid. This point has been discussed as part of the two-fluid model in Chapter 4. As an aside, it is possible to understand physically the invariance to velocity by analogy to an ordinary heat conduction mechanism. In the latter case, heat transported by conduction in a moving medium is no different from that of the medium at rest provided $v \ll c$, the speed of sound. Furthermore, by making the normal set of simplifications to reduce the problem to one-dimensional heat flow in turbulent He II, the nonlinear Gorter–Mellink equation can be used to describe the heat conducted by internal convection,

$$q_{ic} = -\left(\frac{1}{f(T)}\frac{dT}{dx}\right)^{1/3} \tag{5.11}$$

where $f(T)$ is the same temperature-dependent heat conductivity function. The power law dependence of (5.11) has been assumed to be 1/3 although the analysis follows the same procedure if a different coefficient is assumed.

The second assumption is that the heat carried by ordinary convection mechanisms can be described by the flow of enthalpy between two points in the system,

$$q_{fc} = \rho v\, \Delta h \tag{5.12}$$

where $\Delta h = h_1 - h_2$ represents the specific enthalpy difference between temperatures T_1 and T_2, that is, $\Delta h = \int_{T_1}^{T_2} C_p\, dT$. For simplicity (5.12) assumes

the fluid density to be constant, which is a reasonably good approximation for He II.

The above two assumptions lead to an equation that is appropriate for analyzing the temperature profile in forced flow He II. This is achieved by combining differential forms of (5.11) and (5.12) and equating them to the time rate of change of the local enthalpy. The resultant equation is similar to the time-dependent heat equation for static He II except that it contains the extra convection term. In one dimension this expression takes the form

$$\frac{d}{dx}\left[\left(\frac{1}{f}\frac{dT}{dx}\right)^{1/3}\right]-\rho v\frac{dh}{dx}=\rho\frac{dh}{dt} \tag{5.13}$$

Given the boundary conditions for a channel containing He II, it is a straightforward problem to integrate (5.13) and thus determine the temperature profile as a function of flow velocity and time. Unfortunately, this solution requires numerical methods because the equation is nonlinear and the functions such as h and f have rather strong temperature dependencies.

A good approximate solution to the steady-state problem, $dh/dt=0$, can be obtained by assuming constant properties with $\Delta h = C_p \Delta T$. This approximation leads to an exactly soluble differential equation. By making the following change of variables

$$\Theta^* = \frac{T-T_2}{T_1-T_2} \tag{5.14a}$$

$$x^* = \frac{x}{L} \tag{5.14b}$$

and

$$K' = 2\rho C_p v(fL)^{1/3}(T_1-T_2)^{2/3} \tag{5.14c}$$

an exactly soluble form of the Bernoulli equation results,

$$-\frac{d}{dx^*}\left[\left(\frac{d^*\Theta}{dx^*}\right)^{1/3}\right]+\frac{K'}{2}\frac{d\Theta^*}{dx^*}=0 \tag{5.15}$$

which coupled with the appropriate boundary conditions can determine the steady-state temperature in a one-dimensional channel.

The results of this analysis for a channel of length $2L$ with its center at T_1 and ends fixed at T_2 are displayed in Fig. 5.11. The left-hand side of the figure can be interpreted as the case where the velocity of flow is opposite to the heat flow by conduction while the right-hand side refers to these quantities working in parallel. Note that the limitations of this solution are primarily in terms of the temperature dependence of the heat capacity C_p

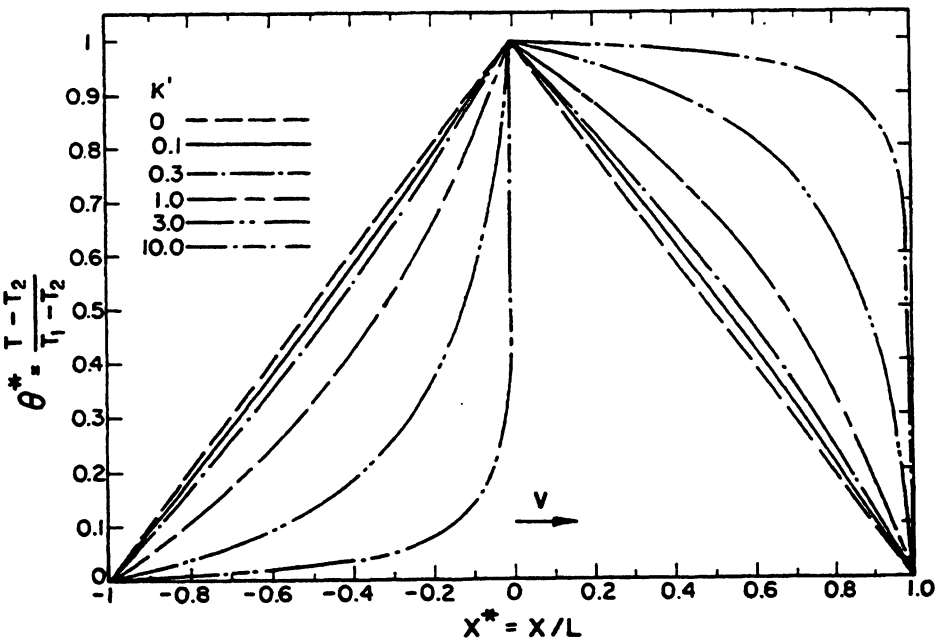

Fig. 5.11. Normalized temperature distribution in forced flow He II with fixed temperature boundary conditions $K' = 2\rho C_p v(fL)^{1/3} (T_1 - T_2)^{2/3}$.

and heat conductivity function $f(T)$. The solution should be quite good for small $\Delta T = T_1 - T_2$ such that $\Delta T/T \ll 1$. The impact of this approximation is seen in the zero velocity profile ($K' = 0$) which is linear, while in fact for large ΔT the profile has considerable curvature. Also note that the nonzero velocity profiles for positive and negative K' are symmetric about the line corresponding to $K' = 0$.

There have been several reports of measured temperature profiles within forced flow He II which have been compared to numerical analyses based on the theory described above.[5.18] In general, these measurements have shown temperature profiles analogous to those displayed in Fig. 5.11. The numerical analysis is more exact because it includes the temperature dependence of the helium properties.

Given the solution to the temperature profile it is straightforward to determine the total heat transport, $q = q_{fc} + q_{ic}$, by integration of (5.15). This result can be normalized to the form

$$\frac{q}{q_0} = -\left(\frac{d\Theta^*}{dx^*}\right)^{1/3} + \frac{K'}{2}\Theta^* \tag{5.16}$$

where K' is defined above and

$$q_0 \equiv \left(\frac{T_1 - T_2}{fL}\right)^{1/3} \tag{5.17}$$

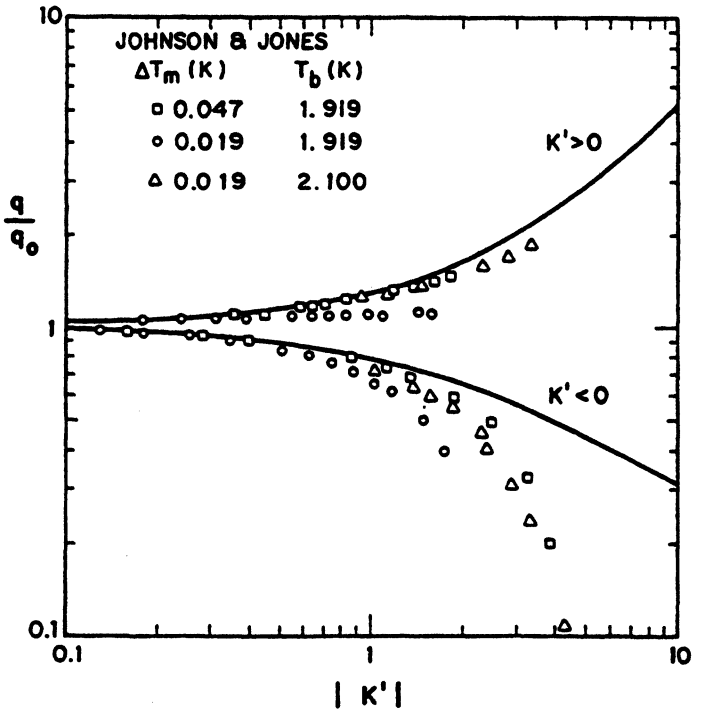

Fig. 5.12. Normalized peak heat flux for forced flow He II with $K' = 2\rho C_p v(fL)^{1/3}(T_1 - T_2)^{2/3}$.

which represents the heat carried by the internal convection mechanisms for He II having zero velocity ($K' = 0$). The results of this calculation are shown by the solid curves in Fig. 5.12. Although there is considerable enhancement of heat transport in the direction of flow even for small K', values of K' greater than unity are required before the total heat transport is enhanced significantly in a midpoint heated channel of length $2L$. This result occurs because forced flow suppresses the total heat transport when the velocity and heat flux are antiparallel.

Johnson and Jones[19] have carried out an extensive investigation of heat transport in saturated forced flow He II. In their experiment a pressure difference was maintained by adjusting the relative height of the two baths. Results obtained required sizable corrections because temperature differences in saturated He II produce a corresponding pressure difference. A comparison of data and analyses is displayed in Fig. 5.12. Although the general trends appear correct, there is considerable discrepancy between the experimental data and theory, particularly for the cases where ΔT is small. A more recent work by Kashani and Van Sciver[18] has shown much closer agreement between theory and the experimental maximum heat flux.